Transverse electric form factors for electron scattering and violation of current conservation in nuclear models

S. Karataglidis, P. Halse, and K. Amos
School of Physics, University of Melbourne, Parkville, Victoria 3052, Australia
(Received 29 July 1994)

Comparison is made between calculations of transverse electric form factors using the standard expression for the electric multipole operator and those obtained by invoking current conservation in the long wavelength limit and for arbitrary momentum transfer. In all cases, only the free-nucleon one-body current and charge operators are explicitly used. Results are presented for select $E2$ transitions in ^{12}C, ^{20}Ne, ^{24}Mg, and ^{28}Si. It is found that the form factors yielded by the various operators differ significantly when the conventional $0\hbar\omega$ shell model wave functions are used, confirming that these do violate conservation of the usual free-nucleon current. For these cases, the data are best reproduced using the operator with current conservation invoked in the long-wavelength limit. However, the variation between results is much smaller when multishell models of nuclear structure are used, all three forms of the operator yielding good agreement with existing data, suggesting that the wave functions obtained from these still practicable models are significantly closer to being current conserving.

PACS number(s): 25.30.Dh, 21.60.Cs, 21.60.Jz

I. INTRODUCTION

Comparisons between calculated and measured longitudinal and transverse electron scattering form factors have long been used as stringent tests of models of nuclear structure. However, while the electromagnetic interaction is known, there is still some uncertainty with regard to the appropriate form of the nuclear currents that are required in analyses of form factors. In particular, the current density (and the charge density) contain in principle one-, two-, up to A-body components, corresponding to the exchange of charged bosons responsible for the nuclear interaction. Analyses of data have usually involved a restriction to just the one-body terms, although some recent analyses of intermediate-energy photonuclear reaction data, for which magnetic interactions are important, have found it necessary to include in the current operator two-body components from meson exchange currents [1], and meson exchange corrections have also been used for magnetic electron scattering [2]. However, because of an incomplete knowledge of the nuclear interaction, the form of the relevant meson exchange currents is not specified with any certainty. Moreover, the most successful structure calculations use phenomenologically determined interactions specified only by matrix elements in a highly truncated basis, which contain insufficient information for a consistent current to be uniquely constructed. An additional problem with form factor analyses in shell model calculations is that, by using a truncated Hilbert space, the resultant wave functions may not satisfy conservation of the nucleon current itself if the usual free-nucleon one-body operator is assumed. As all practical nuclear shell model calculations involve truncated basis spaces and, in most cases, interactions specified only by matrix elements, the problem arises as to what operator specification should be used for obtaining form factors that is both practicable and capable of an accurate reproduction of the data. In the case of the electric multipoles, the difficulties discussed above may be partially circumvented by the use of Siegert's theorem, with which one can replace the current density by the charge density in such a way that the effects of omitted currents are incorporated implicitly [3]. The limitation in the form of the electric transition operator is then that associated with the charge density, of order $(v/c)^2$, rather than of order (v/c) as is the case with the current density [4].

Friar and Haxton [4] and Friar and Fallieros [5] derived alternative forms for the transverse electric operator by invoking current conservation, via Siegert's theorem, either in the long-wavelength limit [4] or for arbitrary wavelength [5]. (There are other forms given in the literature: See, for example, Eisenberg and Greiner [6], Foldy [7], and Rose [8].) Numerical results were limited to the $0^+_{\rm g.s.} \rightarrow 2^+_1;0$ and the $0^+_{\rm g.s.} \rightarrow 2^+_1;1$ transitions in ^{12}C, with wave functions obtained from a p-shell model calculation in which the Cohen-Kurath interaction [9] was used. It was found [4] that the three operators considered gave markedly different form factors, thus implying that the p-shell model wave functions indeed did not give current conservation. Use of the hybrid forms of the operator gave better agreement with the data but Friar and Haxton [4] concluded that these forms were still inappropriate, as that agreement did not extend over the whole range of momentum transfer measured. However, the same wave functions also gave a longitudinal form factor for scattering to the $2^+_1;0$ state that was a factor of 2 smaller than the measured result, so suggesting further investigation of current conservation with wave functions that do give a good reproduction of that longitudinal form factor.

Gmitro *et al.* [10] have also studied these transitions in ^{12}C. They include the constraints imposed by current

conservation, and studied several derivations of the transverse electric operator. Working within the p shell with bare charges and harmonic-oscillator single-particle wave functions, they obtained results similar to those of Friar and Haxton. However, they used different harmonic-oscillator parameters for the two form factors considered, so that while good fits to the data were achieved, their results cannot be used as a reasonable assessment of the different forms of the transverse electric operator.

The extent to which Siegert's theorem can account for the omission of the two ostensibly different sources of current nonconservation in shell model calculations, and indeed the possibility of using it to extract information on the meson exchange currents given explicit cross shell currents, remains to be thoroughly investigated. The purpose of this paper is to present investigations for a range of nuclei in the p and sd shells with both $0\hbar\omega$ and large basis models of nuclear structure. Form factors found using different expressions of the electric multipole operator, but only the usual free-nucleon current and charge operators, will thus be compared over a larger sample of cases than used to date, including transitions for which explicit core polarization amplitudes have been defined.

II. CALCULATION OF FORM FACTORS

A brief development of the electron scattering form factors is given herein, not only for completeness, but also to identify those elements of nuclear structure that enter analyses and to specify how the diverse forms of the transverse electric operators differ.

Electron scattering form factors involving angular momentum transfer J may be expressed as

$$|F_J^\eta(q)|^2 = \frac{1}{2J_i+1}\left(\frac{4\pi}{Z^2}\right)\left|\left\langle \Psi_{J_f}\left\|T_J^\eta(q)\right\|\Psi_{J_i}\right\rangle\right|^2, \quad (1)$$

where η selects the longitudinal, transverse electric, and transverse magnetic form factors, respectively. Assuming one-body forms for the operators, the reduced matrix elements may be expressed in the form [11]

$$\left\langle \Psi_{J_f}\left\|T_J^\eta(q)\right\|\Psi_{J_i}\right\rangle = \mathrm{Tr}(SM)/(2J+1)^{1/2}, \quad (2)$$

where S is the matrix of transition densities, and M contains the single-particle matrix elements. The reduced transition density matrix elements are designated by

$$S^{(\alpha)}_{j_1 j_2 J} = \left\langle \Psi_{J_f}\left\|\left[a^\dagger_{j_2}\times a_{j_1}\right]^J_{(\alpha)}\right\|\Psi_{J_i}\right\rangle \quad (3)$$

and

$$M^{(\alpha)}_{j_1 j_2 J} = \left\langle \phi^{(\alpha)}_{j_2}\left\|T_J^\eta(q)\right\|\phi^{(\alpha)}_{j_1}\right\rangle, \quad (4)$$

where α is the particle label. In these calculations, the single-particle wave functions $\{\phi_j^{(\alpha)}\}$ are of harmonic-oscillator form.

For calculations of the longitudinal form factor we have used the one-body charge operator of deForest and Walecka [12]. Using essentially the notation of Friar and Haxton [4], the one-body transverse electric operator is defined by [4,12]

$$T^{\mathrm{el}(1)}_{JM}(q) = f_{SN}(q_\mu^2)\frac{q}{2M}\sum_{k=1}^{A}\left\{\Delta_{JM}(k)[1+\tau_3(k)] + \Sigma_{JM}(k)\frac{1}{2}[\mu^s+\mu^v\tau_3(k)]\right\}, \quad (5)$$

where

$$\Delta_{JM}(k) = \left[-\sqrt{\frac{J}{2J+1}}\mathbf{M}^M_{JJ+1}(q\vec{r}_k) + \sqrt{\frac{J+1}{2J+1}}\mathbf{M}^M_{JJ-1}(q\vec{r}_k)\right]\cdot\frac{1}{q}\nabla(k) \quad (6)$$

and

$$\Sigma_{JM}(k) = \mathbf{M}^M_{JJ}(q\vec{r}_k)\cdot\sigma(k). \quad (7)$$

The functions $M_{JM}(q\vec{r}_k)$ and $\mathbf{M}^M_{JL}(q\vec{r}_k)$ are defined by

$$M_{JM}(q\vec{r}) = j_J(qr)Y_{JM}(\Omega_r) \quad (8a)$$

and

$$\mathbf{M}^M_{JL}(q\vec{r}) = j_L(qr)\mathbf{Y}^M_{JL1}(\Omega_r). \quad (8b)$$

The superscript (1) designates that the charge and current densities used to develop these transition operators were of one-body form, $f_{SN}(q_\mu^2)$ are reduced single-nucleon form factors [4], and $\mu^{(s,v)}(=\mu_p\pm\mu_n)$ are the isoscalar and isovector magnetic moments, 0.88 and 4.706, respectively.

Invoking current conservation, i.e., using

$$\nabla\cdot\vec{j} = -i[H,\rho], \quad (9)$$

at low momentum transfer, gives the form $T^{\mathrm{el}'(1)}_{JM}$ [4], namely,

$$T^{\mathrm{el}'(1)}_{JM}(q) = f_{SN}(q_\mu^2)\left(\sqrt{\frac{J+1}{J}}\left[\frac{q}{2M}+\frac{E_i-E_f}{q}\right]\sum_{k=1}^{A}M_{JM}(k)\frac{1}{2}[1+\tau_3(k)] + \frac{q}{2M}\sum_{k=1}^{A}\left\{\frac{2J+1}{J}\Delta'_{JM}(k)[1+\tau_3(k)]+\Sigma_{JM}(k)\frac{1}{2}[\mu^s+\mu^v\tau_3(k)]\right\}\right), \quad (10)$$

where

$$\Delta'_{JM}(k) = -\sqrt{\frac{J}{2J+1}}\mathbf{M}^M_{JJ+1}(q\vec{r}_k)\cdot\frac{1}{q}\nabla(k)\ . \quad (11)$$

Friar and Fallieros [5] derived a form for the transverse electric operator in which current conservation is invoked for arbitrary wavelength. When using the one-body operators, this operator, denoted by $T^{\mathrm{el}''(1)}_{JM}(q)$, is given by [4]

$$T^{\mathrm{el}''(1)}_{JM}(q) = f_{SN}(q^2_\mu)\Bigg\{\sqrt{\frac{J+1}{J}}\frac{E_i - E_f}{q}\sum_{k=1}^{A} M^g_{JM}(k)\frac{1}{2}[1+\tau_3(k)] + \frac{\sqrt{J(J+1)}}{J+2}\frac{q}{2M}\sum_{k=1}^{A} M^h_{JM}(k)\frac{1}{2}[1+\tau_3(k)] + \frac{2J+3}{J+2}\frac{q}{M}\sum_{k=1}^{A}\Delta''_{JM}(k)\frac{1}{2}[1+\tau_3(k)] + \frac{q}{2M}\sum_{k=1}^{A}\Sigma_{JM}(k)\frac{1}{2}[\mu^s + \mu^v\tau_3(k)]\Bigg\}, \tag{12}$$

where, with $\Sigma_{JM}(k)$ defined by Eq. (7),

$$M^g_{JM}(k) = \frac{(qr_k)^J}{(2J+1)!!}g_J(qr_k)Y_{JM}(\Omega_k),$$

$$M^h_{JM}(k) = \frac{(qr_k)^J}{(2J+1)!!}h_J(qr_k)Y_{JM}(\Omega_k),$$

$$\Delta''_{JM}(k) = -\frac{(qr_k)^{J+1}}{(2J+3)!!}h_J(qr_k)\frac{1}{\sqrt{2J+1}}\left[\sqrt{J}\,\mathbf{Y}^M_{JJ+11}(\Omega_k) + \sqrt{J+1}\,\mathbf{Y}^M_{JJ-11}(\Omega_k)\right]\cdot\frac{\nabla(k)}{q},$$

and

$$g_J(z) = \frac{J(2J+1)!!}{z^J}\int_0^z dy\frac{j_J(y)}{y} = 1 - \frac{Jz^2}{2(J+2)(2J+3)} + \cdots,$$

$$h_J(z) = -\left(\frac{J+2}{Jz}\right)\frac{d}{dz}\frac{1}{z^{2J}}\frac{d}{dz}\left[z^{2J+1}g_J(z)\right] = 1 - \frac{(J+2)z^2}{2(J+4)(2J+3)} + \cdots.$$

Using this last form of the operator in an analysis of the transverse $E2$ form factor for the 2^+ (4.44 MeV) state in ^{12}C, Friar and Haxton [4] found that the calculated form factor had an incorrect high-q dependence. This they attributed to an unphysical singularity in the Siegert-like part of the current density operator which contributed significantly because the nuclear wave functions did not give current conservation; with wave functions that give current conservation, any contribution from that singularity is canceled by a corresponding term from the magnetic moment current density [4]. Indeed, the three operator forms, related by the assumption of current conservation, will by construction give identical matrix elements if a consistent system of wave functions and corresponding conserved charge-current operators is used. However, in practical nuclear structure calculations the free-nucleon one-body current and restricted space basis states do not form such a consistent system; effective two-body currents would have to be generated to account for the omission of meson exchange, corresponding to the actual nuclear interaction, and for the omission of basis states outside the assumed space. The main question we address, in the context of practical calculations, is which, if any, of the three forms allows a consistently accurate description of electric form factors when the simple free-nucleon current is used with practicable wave functions.

Hereafter, for simplicity, the multipole subscripts, mark (1) superscript, and momentum transfer variable will be omitted in reference to the transverse electric operators.

III. RESULTS

Electron scattering form factors from the $0^+ \rightarrow 2^+_1$ isoscalar transitions in ^{12}C (4.44 MeV), ^{20}Ne (1.63 MeV), ^{24}Mg (1.37 MeV), and ^{28}Si (1.78 MeV), as well as the $0^+ \rightarrow 2^+_1$ isovector transition in ^{12}C (16.11 MeV), have been evaluated using transition densities calculated in the shell model (for all transitions) using the program OXBASH [13], and also by using projected Hartree-Fock (PHF) wave functions [14] in the case of ^{20}Ne, ^{24}Mg, and ^{28}Si. The Cohen-Kurath (8-16)2BME interaction [9] was used to give p-shell model wave functions for ^{12}C. We have also used full $(0+2)\hbar\omega$ wave functions for ^{12}C which were calculated using the MK3W interaction supplied with OXBASH. Likewise, sd-shell model wave functions were determined for ^{20}Ne, ^{24}Mg, and ^{28}Si with the W interaction of Wildenthal as supplied with OXBASH [13]. The transition density matrix elements for all reactions considered are given in five tables and will be discussed subsequently as we consider each form factor in turn. In all these tables we have used the nomenclature of Amos and Steward [11] to specify the individual particle orbits j_1 and j_2. Bare charges were used in all calculations.

A. p-shell nucleus: ^{12}C

Table I lists the transition densities for the $0^+ \rightarrow 2^+$ (4.44 MeV) transition in ^{12}C obtained using both the p-shell model wave functions and the full $(0+2)\hbar\omega$ shell model wave functions. The transition densities obtained from the full $(0+2)\hbar\omega$ shell model wave functions agree almost entirely with the projected Hartree-Fock transition densities of Amos and Morrison [15], the PHFBA set. The advantage of using these large basis shell model wave functions over the PHF wave functions is then that the transition densities for the isovector 2^+ transition (16.11 MeV) in ^{12}C may also be obtained. The effect of increasing the basis is evident from this table. The slight increase in the $p_{\frac{3}{2}}$ shell recoupling amplitude is offset by the decrease in the $p_{\frac{3}{2}} \rightarrow p_{\frac{1}{2}}$ transition. The effect of this increase in basis is illustrated by the longitudinal $E2$ form factor from electron scattering to this state. The measured longitudinal form factor [16] is displayed in Fig. 1, and is compared with our p-shell model and $(0+2)\hbar\omega$ shell model calculations, in which a harmonic-oscillator length of 1.7 fm was used. It is the inclusion of the other transitions, notably those involving the $0s$ shell, which gives nearly exact agreement with experiment. This improvement in the description of the longitudinal form factor is also reflected in the transverse $E2$ form factor.

The transverse electric form factor from electron scattering to this 2^+ state has been measured [16], and those data are compared with the results of our diverse calculations in Fig. 2. The p-shell model and the $(0+2)\hbar\omega$ results are displayed in Figs. 2(a) and 2(b), respectively. In both segments, the solid, dotted, and dashed curves depict the results of calculations made using the $T^{\rm el}$, $T^{\rm el'}$, and $T^{\rm el''}$ operators, respectively.

Clearly there is a significant improvement in the fits to the data by changing from the standard $T^{\rm el}$ operator to $T^{\rm el'}$, confirming the result of Friar and Haxton [4]. The effect is particularly significant at low q, where meson exchange currents are expected to be negligible, indicating that the $T^{\rm el'}$ operator corrects for the lack of cross shell nucleonic currents within the p-shell model. With the bigger basis calculation [Fig. 2(b)] the effect of replacing $T^{\rm el}$ by $T^{\rm el'}$ is not as dramatic, presumably because some of the cross shell currents are now included explicitly. Rather the correction is essentially just a scale shift. The shift is not sufficient to fit the measured data, for which a further enhancement of 1.6 in the result using $T^{\rm el'}$ would be required to bring about agreement over the whole range of momentum transfer.

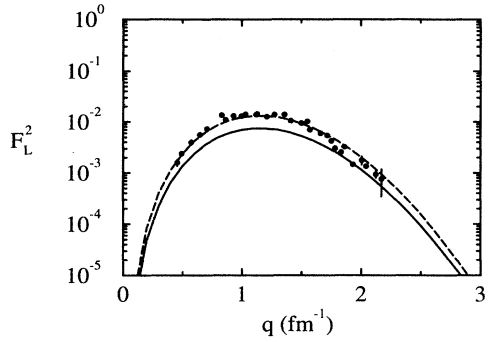

FIG. 1. The longitudinal form factor from the isoscalar 2^+ (4.44 MeV) transition in ^{12}C. The data of Flanz *et al.* [16] are compared to the result of the p-shell model calculation (solid curve) and to the result of the calculation made using the full $(0+2)\hbar\omega$ shell model wave functions (dashed curve).

TABLE I. Transition density matrix elements for the $0^+ \rightarrow 2^+$ (4.44 MeV) excitation in ^{12}C. The nomenclature for the $j_1 : j_2$ coupling is as used in Table I of Ref. [11]. Proton and neutron transition matrix elements are identical.

$0p$			$1s0d$				$0f1p$	
$j_1 : j_2$	$S_{j_1 j_2}$ [a]	$S_{j_1 j_2}$ [b]	$j_1 : j_2$	$S_{j_1 j_2}$	$j_1 : j_2$	$S_{j_1 j_2}$	$j_1 : j_2$	$S_{j_1 j_2}$
2:2	0.5609	0.5020	1:4	−0.1586	2:7	−0.1391	8:8	−0.0007
2:3	−1.0706	−1.1956	1:5	0.1356	2:8	0.0530	8:9	−0.0001
3:2	0.7728	0.7735	4:1	−0.1124	2:9	−0.0136	8:10	−0.0004
			4:4	0.0174	2:10	0.0270	9:2	0.0093
			4:5	−0.0060	3:8	−0.0526	9:3	−0.0042
			4:6	0.0026	3:9	0.0003	9:7	−0.0011
			5:1	−0.0949	7:2	−0.0576	9:8	0.0007
			5:4	0.0042	7:7	−0.0038	9:9	0.00005
			5:5	0.0087	7:8	0.0010	9:10	0.00008
			5:6	0.0012	7:9	−0.0008	10:2	0.0055
			6:4	0.0013	8:2	−0.0398	10:8	−0.0004
			6:5	−0.0016	8:3	−0.0071	10:9	0.00008
					8:7	−0.0020		

[a] $(0+2)\hbar\omega$ shell model.
[b] p-shell model.

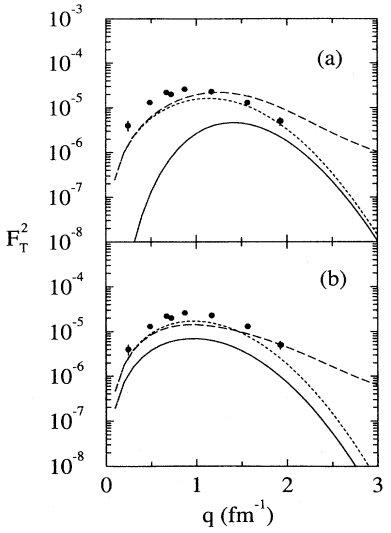

FIG. 2. The transverse isoscalar $E2$ form factor for the 4.44 MeV transition in ^{12}C. The data are those of Flanz *et al.* [16]. (a) Comparison with p-shell calculations, the solid, dotted, and dashed lines depicting the results of using $T^{\rm el}$, $T^{\rm el'}$ and $T^{\rm el''}$ operators. (b) Comparison with form factors calculated using the $(0+2)\hbar\omega$ shell model wave functions with $T^{\rm el}$ (solid curve), $T^{\rm el'}$ (dotted curve), and $T^{\rm el''}$ (dashed curve).

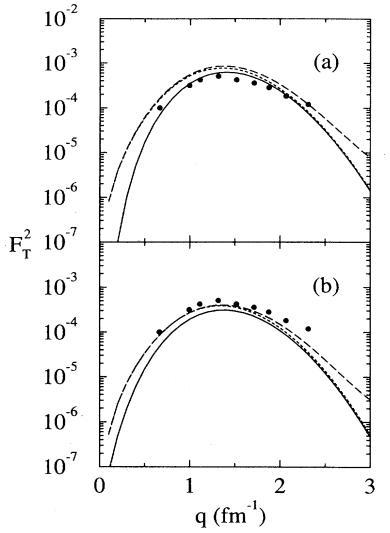

FIG. 3. The transverse $E2$ form factor for the isovector $0^+ \rightarrow 2^+$ (16.11 MeV) transition in ^{12}C. The data of Flanz *et al.* [16] are compared to the calculations using $T^{\rm el}$ (solid curve), $T^{\rm el'}$ (dotted curve), and $T^{\rm el''}$ (dashed curve). In (a) is displayed the results found using p-shell model wave functions, while in (b) the results shown were obtained using the $(0+2)\hbar\omega$ shell model wave functions.

The results using $T^{\rm el''}$ indicate the same anomalous behavior at high momentum transfer shown in the calculations of Friar and Haxton [4], although more data at $q \sim 2-3$ fm^{-1} are needed to confirm this observation. There is improvement in the low-q part of the form factor, but this is the same as for $T^{\rm el'}$, as the two operators necessarily give the same matrix elements in the long-wavelength limit. While there is improvement in the $T^{\rm el''}$ calculation when the $(0+2)\hbar\omega$ wave functions are employed, the dependence on q is still markedly different from that for $T^{\rm el}$ and $T^{\rm el'}$. The anomalous behavior at high momentum transfer, and indeed differences in the three curves for all q, indicates that even the complete $(0+2)\hbar\omega$ wave functions we have used do not give complete conservation of the assumed one-body nuclear current, although the violation is much less than with the

TABLE II. Proton transition density matrix elements for the $0^+ \rightarrow 2^+$ (16.11 MeV) transition in ^{12}C. The matrix elements for the neutron transitions are the negative of the proton matrix elements.

$0p$			$1s0d$		$0f1p$			
$j_1:j_2$	$S_{j_1j_2}$[a]	$S_{j_1j_2}$[b]	$j_1:j_2$	$S_{j_1j_2}$	$j_1:j_2$	$S_{j_1j_2}$	$j_1:j_2$	$S_{j_1j_2}$
2:2	0.1409	0.0749	1:4	−0.0033	2:7	−0.0037	8:8	−0.0012
2:3	0.9446	1.0898	1:5	0.0101	2:8	0.0381	8:9	−0.0011
3:2	−0.2129	−0.1784	4:1	−0.0212	2:9	−0.0096	8:10	0.00005
			4:4	−0.0013	2:10	−0.1185	9:2	0.0067
			4:5	−0.00001	3:8	0.0225	9:3	0.0038
			4:6	0.0029	3:9	0.0350	9:7	−0.00009
			5:1	0.0030	7:2	−0.0573	9:8	−0.00008
			5:4	0.0013	7:7	−0.0016	9:9	−0.0003
			5:5	0.0012	7:8	0.0027	9:10	−0.0004
			5:6	−0.0010	7:9	0.0069	10:2	0.0024
			6:4	−0.0004	8:2	0.0114	10:8	0.0004
			6:5	−0.0006	8:3	−0.0020	10:9	0.0003
					8:7	−0.0011		

[a] $(0+2)\hbar\omega$ shell model.
[b] p-shell model.

simple p-shell model.

The isovector $E2$ form factor from inelastic electron scattering to the 16.11 MeV 2^+ state in ^{12}C has also been measured [16] and is of interest as past studies suggest that the Cohen-Kurath wave functions give a good specification of the transition [16,4]. The relevant 2^+ isovector transition density matrix elements are given in Table II for both the p-shell and the $(0+2)\hbar\omega$ shell model calculations. With this transition, the larger basis structure calculation modulates the p-shell components from the values they have with the small basis model, and compensates with numerous small additional elements. But, unlike the case with the isoscalar 4.44 MeV transition, only the $0p \leftrightarrow (0f1p)$ elements are nontrivial. The net effect is that core polarization effects in this isovector excitation, as measured by the variation in the form factors when the p shell and $(0+2)\hbar\omega$ shell model wave functions are used, are not as dramatic as with the isoscalar excitation. Indeed, they are destructive in nature as is evident from the calculated form factors that are displayed in Fig. 3, where the line types refer to the three operators as for Fig. 2. The p-shell calculations are contained in Fig. 3(a) while those found using the $(0+2)\hbar\omega$ wave functions are given in Fig. 3(b). In the case of the p-shell results, the calculation using the $T^{\rm el}$ operator is in best agreement with the data. This is not the case in the calculations using the large basis wave functions, as then the calculations made using both the $T^{\rm el'}$ and $T^{\rm el''}$ operators are in better agreement with the data.

B. *sd*-shell nuclei: ^{20}Ne, ^{24}Mg, and ^{28}Si

The isoscalar $E2$ form factors from inelastic electron scattering to the 1.37 MeV state of ^{24}Mg have been measured [17], and for these as well as the form factors for the $0^+ \rightarrow 2^+$ transitions in ^{20}Ne (1.63 MeV) and ^{28}Si (1.78 MeV) both the *sd*-shell model and large basis PHF model transition densities [14] have been obtained. (The PHF transition densities for ^{20}Ne and ^{24}Mg have been published previously [18,11], but are included here for comparison to the *sd*-shell model transition densities, and also to correct several inconsistencies contained in the previous publications.) Clearly from Tables III, IV, and V there are significant contributions involving transitions other than those within the *sd* shell. In all cases, the large basis PHF spectroscopy markedly changes some of the *sd*-shell values from those of the small basis shell model, and particularly for the transition in ^{28}Si. In addition there are numerous additional elements in the PHF

TABLE III. Transition densities for the $0^+ \rightarrow 2^+$ (1.37 MeV) transition in ^{24}Mg deduced from *sd*-shell and large basis PHF structure calculations. Proton and neutron transition matrix elements are identical.

	$1s0d$		$0f1p$		$0g2s1d$			
$j_1:j_2$	$S_{j_1j_2}$[a]	$S_{j_1j_2}$[b]	$j_1:j_2$	$S_{j_1j_2}$	$j_1:j_2$	$S_{j_1j_2}$	$j_1:j_2$	$S_{j_1j_2}$
4:4	0.8308	0.9765	2:7	−0.2270	1:13	−0.0611	13:5	−0.0956
4:5	−0.5738	−0.4987	2:8	0.1054	1:14	0.0497	13:6	0.1084
4:6	0.6818	0.6729	2:9	−0.0368	4:11	−0.1918	13:11	−0.0320
5:4	0.5954	0.5055	2:10	0.0302	4:12	0.0761	13:12	0.0126
5:5	−0.0151	0.1033	3:8	−0.2169	4:13	0.1419	13:13	0.0243
5:6	0.1969	0.2407	3:9	−0.0377	4:14	−0.0517	13:14	−0.0089
6:4	0.5428	0.5110	7:2	−0.1762	4:15	0.1530	13:15	0.0239
6:5	−0.2321	−0.2329	7:7	0.0127	5:12	−0.0396	14:1	−0.0390
			7:8	−0.0047	5:13	0.0980	14:4	0.0536
	$0s \leftrightarrow 1s0d$		7:9	−0.0464	5:14	0.0015	14:5	0.0007
			8:2	−0.0819	5:15	0.0436	14:6	0.0110
1:4	−0.1641		8:3	−0.1685	6:13	0.0844	14:12	−0.0037
1:5	0.1229		8:7	0.0046	6:14	−0.0129	14:13	0.0091
2:2	0.0160		8:8	0.0160	11:4	−0.1203	14:14	0.0009
2:3	−0.0130		8:9	−0.0216	11:11	0.0102	14:15	0.0020
3:2	0.0132		8:10	−0.0368	11:12	−0.0039	15:4	0.1218
4:1	−0.2092		9:2	−0.0274	11:13	−0.0202	15:5	−0.0514
5:1	−0.1027		9:3	0.0283	12:4	−0.0531	15:13	0.0184
			9:7	−0.0602	12:5	−0.0277	15:14	−0.0023
			9:8	0.0280	12:11	0.0046		
			9:9	−0.0178	12:12	0.0032		
			9:10	0.0146	12:13	−0.0098		
			10:2	−0.0226	12:14	−0.0026		
			10:8	−0.0476	13:1	−0.0608		
			10:9	−0.0147	13:4	0.1403		

[a]PHF.
[b]Shell model.

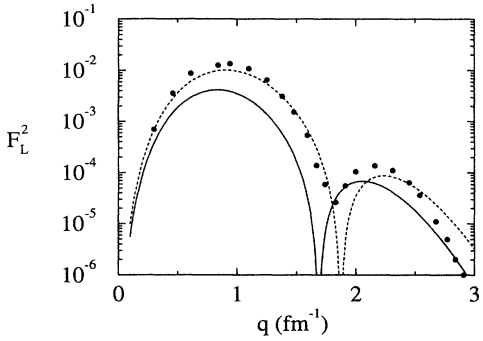

FIG. 4. The longitudinal $E2$ form factor for the $0^+ \rightarrow 2^+$ (1.37 MeV) transition in ^{24}Mg. The data of Hotta *et al.* [17] are compared with the results of calculations made using *sd*-shell model and PHF wave functions that are shown by the solid and dotted curves, respectively.

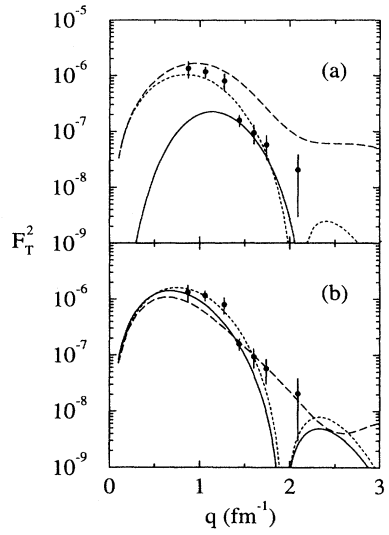

FIG. 5. The transverse $E2$ form factor for the $0^+ \rightarrow 2^+$ (1.37 MeV) transition in ^{24}Mg. The data of Hotta *et al.* [17] are compared with the results of calculations made using the T^{el} operator (solid line), the $T^{el'}$ operator (dotted line), and the $T^{el''}$ operator (dashed line). The results presented in (a) were found by using *sd*-shell model wave functions while those given in (b) were obtained by using PHF wave functions.

set and many are nontrivial. Matrix elements involving all of the basis ($0s \rightarrow 0g1d2s$) orbits are needed and some are even more significant than the smallest purely *sd*-shell elements. In the calculations of the form factors made using these transition density matrix elements, harmonic-oscillator lengths of 1.8 fm, 1.9 fm, and 2.0 fm

TABLE IV. Transition densities for the $0^+ \rightarrow 2^+$ (1.63 MeV) transition in ^{20}Ne deduced from *sd*-shell and large basis PHF structure calculations. Proton and neutron transition matrix elements are identical.

	$1s0d$		$0f1p$		$0g2s1d$			
$j_1 : j_2$	$S_{j_1 j_2}$[a]	$S_{j_1 j_2}$[b]	$j_1 : j_2$	$S_{j_1 j_2}$	$j_1 : j_2$	$S_{j_1 j_2}$	$j_1 : j_2$	$S_{j_1 j_2}$
4:4	−0.5919	−0.6340	2:7	0.1743	1:13	0.0352	13:5	0.0144
4:5	0.1693	0.1631	2:8	−0.0887	1:14	−0.0256	13:6	−0.0467
4:6	−0.6015	−0.5940	2:9	0.0577	4:11	0.1006	13:11	0.0085
5:4	−0.1213	−0.1394	2:10	−0.0491	4:12	−0.0216	13:12	−0.0018
5:5	−0.1066	−0.1497	3:8	0.1803	4:13	−0.0497	13:13	−0.0043
5:6	−0.1931	−0.2424	3:9	0.0601	4:14	0.0056	13:14	0.0006
6:4	−0.7522	−0.6956	7:2	0.1307	4:15	−0.0458	13:15	−0.0029
6:5	0.3413	0.3443	7:7	−0.0083	5:12	0.0268	14:1	0.0187
			7:8	0.0037	5:13	−0.0103	14:4	−0.0041
	$0s \leftrightarrow 1s0d$		7:9	0.0265	5:14	−0.0039	14:5	−0.0039
			8:2	0.0666	5:15	−0.0132	14:6	−0.0023
1:4	0.1903		8:3	0.1353	6:13	−0.0582	14:12	0.0010
1:5	−0.1277		8:7	−0.0040	6:14	0.0058	14:13	−0.0004
2:2	−0.0151		8:8	−0.0116	11:4	0.0468	14:14	−0.0003
2:3	0.0047		8:9	0.0136	11:11	−0.0051	14:15	0.0007
3:2	−0.0062		8:10	0.0179	11:12	0.0010	15:4	−0.0570
4:1	0.1481		9:2	0.0424	11:13	0.0039	15:5	0.0240
5:1	0.0810		9:3	−0.0449	12:4	0.0057	15:13	−0.0035
			9:7	0.0348	12:5	0.0100	15:14	−0.0007
			9:8	−0.0180	12:11	−0.0006		
			9:9	0.0216	12:12	−0.0015		
			9:10	−0.0164	12:13	0.0005		
			10:2	0.0364	12:14	0.0004		
			10:8	0.0237	13:1	0.0268		
			10:9	0.0158	13:4	−0.0497		

[a]PHF.
[b]Shell model.

were used for ^{20}Ne, ^{24}Mg, and ^{28}Si, respectively.

Our results for the longitudinal form factor from inelastic scattering to the 2^+ (1.37 MeV) state in ^{24}Mg are compared in Fig. 4 with the data of Hotta *et al.* [17]. The *sd*-shell model and PHF results are displayed by the solid and dotted lines, respectively. In the case of the PHF calculation, we stress that the numerous small elements beyond the *sd* shell were important in giving the quality of fit to the data, notably by yielding a momentum variation in addition to an enhancement in strength upon the *sd*-shell model form factor. Such an effect in 2^+ excitations via inelastic pion scattering also improved agreement with the measured data [19].

The transverse $E2$ form factor from scattering to the 2^+ (1.37 MeV) state was also measured by Hotta *et al.* [17], and in Fig. 5 those data are compared with our calculated form factors. In Fig. 5(a), *sd*-shell model results are given while in Fig. 5(b) the large basis PHF results are shown. In both cases, the solid, dotted, and dashed curves portray the form factors calculated using the $T^{\rm el}$, $T^{\rm el'}$, and $T^{\rm el''}$ operators, respectively. The effect of changing from the $T^{\rm el}$ operator to the modified operators with the *sd*-shell model wave functions is dramatic. Considerable improvement is apparent for low q with either the $T^{\rm el'}$ or $T^{\rm el''}$ operators, although the calculation using the latter exhibits the same undesirable behavior at high momentum transfer as did the form factors for ^{12}C.

The significant enhancement in the *sd*-shell model form factor at low-q values when the modified operators are used, and in the $T^{\rm el}$ form factor on going to the large basis PHF wave functions, indicates the marked nonconservation of the assumed one-body nuclear current with the *sd*-shell model wave functions. In contrast, the relatively small differences between results arising from all three operators with the PHF structure suggest that with those wave functions current conservation is more nearly satisfied. As for ^{12}C, the low-q part is verified to be given almost entirely by currents involving excitation between major shells.

Differences in the calculations using the three transverse electric operators are most evident in the calculations of the isoscalar $E2$ form factor for scattering to the 2^+ (1.63 MeV) state in ^{20}Ne. Our calculations using the transition densities given in Table IV are displayed in Fig. 6, wherein the solid curves are the *sd*-shell model calculations and the dashed curves are those calculations performed with the PHF wave functions. In the calculations using the $T^{\rm el}$ operator there is a dramatic difference between the *sd*-shell model and PHF calculations. The effect of core polarization is to introduce a minimum in the form factor at 1.25 fm^{-1}, which is not present in the

TABLE V. Transition densities for the $0^+ \rightarrow 2^+$ (1.78 MeV) transition in ^{28}Si deduced from *sd*-shell and large basis PHF structure calculations. Proton and neutron transition matrix elements are identical.

$1s0d$			$0f1p$		$0g2s1d$			
$j_1 : j_2$	$S_{j_1 j_2}$[a]	$S_{j_1 j_2}$[b]	$j_1 : j_2$	$S_{j_1 j_2}$	$j_1 : j_2$	$S_{j_1 j_2}$	$j_1 : j_2$	$S_{j_1 j_2}$
4:4	0.7088	0.4722	2:7	−0.2074	1:13	−0.0801	13:5	−0.1470
4:5	−0.6542	−0.6064	2:8	0.1001	1:14	0.0517	13:6	0.1144
4:6	0.6331	0.9406	2:9	−0.0393	4:11	−0.0456	13:11	−0.0087
5:4	0.6111	0.4804	2:10	0.0287	4:12	0.0421	13:12	0.0091
5:5	0.4549	0.2709	3:8	−0.1864	4:13	0.1658	13:13	0.0379
5:6	0.1481	0.1363	3:9	−0.0318	4:14	−0.1130	13:14	−0.0249
6:4	0.6782	0.6428	7:2	−0.1659	4:15	0.1514	13:15	0.0271
6:5	−0.2865	−0.2422	7:7	−0.0108	5:12	−0.0432	14:1	−0.0375
			7:8	0.0044	5:13	0.1386	14:4	0.1060
	$0s \leftrightarrow 1s0d$		7:9	−0.0456	5:14	0.0764	14:5	0.0787
			8:2	−0.0802	5:15	0.0351	14:6	−0.0032
1:4	−0.2475		8:3	−0.1492	6:13	0.1185	14:12	−0.0063
1:5	0.1541		8:7	−0.0044	6:14	−0.0099	14:13	0.0236
2:2	0.0183		8:8	−0.0125	11:4	−0.0296	14:14	0.0123
2:3	−0.0143		8:9	−0.0217	11:11	−0.0041	14:15	−0.0011
3:2	0.0146		8:10	−0.0346	11:12	0.0031	15:4	0.1621
4:1	−0.2250		9:2	−0.0303	11:13	−0.0058	15:5	−0.0681
5:1	−0.0950		9:3	0.0246	12:4	−0.0296	15:13	0.0280
			9:7	−0.0565	12:5	−0.0181	15:14	−0.0020
			9:8	0.0270	12:11	−0.0046		
			9:9	−0.0208	12:12	−0.0008		
			9:10	0.0149	12:13	−0.0064		
			10:2	−0.0221	12:14	−0.0026		
			10:8	−0.0430	13:1	−0.0698		
			10:9	−0.0148	13:4	0.1654		

[a]PHF.
[b]Shell model.

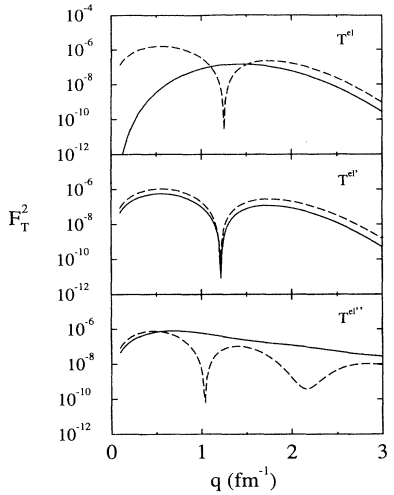

FIG. 6. Calculated results for the transverse $E2$ form factor for the $0^+ \rightarrow 2^+$ (1.63 MeV) transition in ^{20}Ne. The solid and dashed curves are for the *sd*-shell model and PHF wave functions, respectively. The operators used are as indicated.

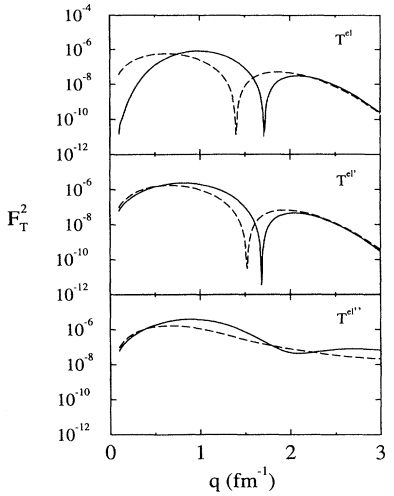

FIG. 7. Calculated results for the transverse $E2$ form factor for the $0^+ \rightarrow 2^+$ (1.78 MeV) transition in ^{28}Si. The curves presented are as for Fig. 6, and the operators used are as indicated.

calculation using the simple *sd*-shell model wave functions. This minimum is also present in both calculations using the $T^{el'}$ operator. In this case, the effect of core polarization is small and the similarity between these calculations and that using the T^{el} operator with PHF wave functions indicates that the $T^{el'}$ operator compensates for any deficiencies in the *sd*-shell model wave functions. Again, it is seen that the *sd*-shell model wave functions do not give current conservation, and the similarities between all three calculations at low q using the PHF wave functions indicate that with these wave functions current conservation is more nearly satisfied. However, unlike the calculations using T^{el} and $T^{el'}$, there is a second minimum at $q = 2.2$ fm^{-1} in the form factor calculated using $T^{el''}$. This is due to cancellation occurring between contributions from the diverse terms of Eq. (12) at this value of momentum transfer.

The *sd*-shell model and large basis PHF transition density matrix elements for the excitation of the 2^+ (1.78 MeV) state in ^{28}Si are given in Table V. They were used in calculations of the transverse electric form factor, the results of which are shown in Fig. 7. The results found using the *sd*-shell model wave functions (solid curve) and PHF wave functions (dashed curve) and for each operator are as indicated. There are similarities between these form factors and those for the transverse electric form factors in ^{24}Mg and ^{20}Ne. However, for ^{28}Si, the PHF results do not conserve the assumed current as well as do those structures for the other two nuclei, as is evident by the low-q part of the form factor calculated using $T^{el''}$ not matching those calculated using the T^{el} and $T^{el'}$ forms of the transition operator. We note especially that there is no indication in the calculated $T^{el''}$ form factor of the minimum, at around 1.5 fm^{-1}, which is present in the calculations using the other two operators.

IV. CONCLUSIONS

Transverse electric form factors for transitions in ^{12}C, ^{20}Ne, ^{24}Mg, and ^{28}Si have been calculated using three forms of the electric transition operator: the standard one (T^{el}) and those obtained by invoking current conservation in the long-wavelength limit ($T^{el'}$) and for arbitrary wavelength ($T^{el''}$). In all cases, the free-nucleon one-body charge density and current density operators were used. The form factors were calculated using $0\hbar\omega$ shell model wave functions, as well as full $(0+2)\hbar\omega$ shell model wave functions for ^{12}C, and projected Hartree-Fock wave functions for the *sd*-shell nuclei.

Using the $0\hbar\omega$ model wave functions, the form factors calculated with the three operators show significant differences for all nuclei, confirming the conclusion of Friar and Haxton that such models violate conservation of the usual one-body current to an extent that is significant in this context. Comparison with the data for ^{12}C and ^{24}Mg indicates that $T^{el'}$ is the most appropriate operator for calculating transverse electric form factors with these models. In contrast, using multishell structure models which are still readily implemented, all three operators give similar form factors in the region $q \leq 3$ fm^{-1}, implying that a much less significant violation of current conservation exists with those wave functions. Moreover, these form factors are in good agreement with the data. Indeed, although the form factor calculated using the $T^{el''}$ operator still shows some anomalous high-q behavior, this is restricted to higher values of q than noted previously so that there is no actual inconsistency with existing data. Measurements of the transverse $E2$ form factors to the 1.63 MeV state in ^{20}Ne and to the 1.78 MeV

state in ^{28}Si, as well as additional data for the $E2$ form factor for the 1.37 MeV state in ^{24}Mg, in the range $q \sim 1.5 - 2.5$ fm^{-1}, are needed for the validity of the three operators in such applications to be further assessed.

The largest effect of the Siegert hybridization of the transverse electric operator for $q < 0.5$ fm^{-1}, when used with $0\hbar\omega$ models, evidently is to account for the neglect of cross shell currents, since the meson exchange currents are expected to be negligible in this regime. This conclusion is explicitly confirmed by inspection of the contributions arising from $T^{\rm el}$ in the extended models. Indeed, further extended calculations of this kind, with explicit inclusion of cross shell current up to large $\hbar\omega$, may allow the extraction of the meson exchange current contributions. This would be a useful check on procedures to calculate their contribution to magnetic form factors.

[1] S. Boffi, C. Giusti, F.D. Pacati, and M. Radici, Nucl. Phys. **A564**, 473 (1993); J. Ryckebusch, L. Machenil, M. Vanderhaeghen, and M. Waroquier, Phys. Lett. B **291**, 213 (1992); D.O. Riska, Phys. Rep. **181**, 207 (1989).

[2] J. L. Friar, Ann. Phys. (N.Y.) **104**, 380 (1977).

[3] M. Gari and H. Hebach, Phys. Rep. **72**, 1 (1981).

[4] J. L. Friar and W. C. Haxton, Phys. Rev. C **31**, 2027 (1985).

[5] J. L. Friar and S. Fallieros, Phys. Rev. C **29**, 1645 (1984).

[6] J. M. Eisenberg and W. Greiner, *Nuclear Theory* (North-Holland, Amsterdam, 1970), Vol. 3.

[7] L. Foldy, Phys. Rev. **92**, 178 (1953).

[8] M. E. Rose, *Multipole Fields* (John Wiley, New York, 1955).

[9] S. Cohen and D. Kurath, Nucl. Phys. **73**, 1 (1965).

[10] M Gmitro, T. D. Kaipov, J. Kvasil, and J. Řízek, Czech. J. Phys. B **37**, 1107 (1987).

[11] K. Amos and C. Steward, Phys. Rev. C **41**, 335 (1990).

[12] T. deForest, Jr. and J. D. Walecka, Adv. Phys. **15**, 1 (1966).

[13] OXBASH-MSU (the Oxford-Buenos-Aires-Michigan State University shell model code). A. Etchegoyen, W. D. M. Rae, and N. S. Godwin (MSU version by B. A. Brown, 1986).

[14] W. C. Ford, R. C. Braley, and J. Bar-Touv, Phys. Rev. C **4**, 2099 (1971).

[15] K. Amos and I. Morrison, Phys. Rev. C **19**, 2108 (1979).

[16] J. B. Flanz, R. S. Hicks, R. A. Lindgren, G. A. Peterson, A. Hotta, B. Parker, and R. C. York, Phys. Rev. Lett. **41**, 1642 (1978).

[17] A. Hotta, R. S. Hicks, R. L. Huffman, G. A. Peterson, R. J. Peterson, and J. R. Shepard, Phys. Rev. C **36**, 2212 (1987).

[18] P. Nesci and K. Amos, Nucl. Phys. **A284**, 239 (1977).

[19] K. Amos and L. Berge, Phys. Lett. **127B**, 299 (1983).